Materials Research. 2025; 28:e20240498
DOI: https://doi.org/10.1590/1980-5373-MR-2024-0498

Densification and Resistance of Ta_2O_5 and ZnO Co-doped SnO_2 Ceramic Targets for Low-cost TCO Films of Solar Cells

Ning Jian[a], Jiwen Xu[a,b], Guisheng Zhu[a,b], Fei Shang[a,b], Huarui Xu[a,b]*

[a]*Guilin University of Electronic Technology, Electronical Information Materials and Devices Engineering Research Center of Ministry of Education, 541004, Guilin, China.*
[b]*Guangxi Key Laboratory of Information Materials, 541004, Guilin, China.*

Received: October 31, 2024; Revised: January 26, 2025; Accepted: March 03, 2025

SnO_2-based TCO films can decrease the cost of solar cells, but its corresponding ceramic targets are difficult to sintering densification. Therefore, Ta_2O_5 and ZnO are used to enhance the density and conductivity of targets. The targets have rutile phase structure, dense microstructure and fine grains. The 0.85 wt% ZnO and 3 wt% Ta_2O_5 doped target sintered at 1500 °C achieve high relative density (>99%) and low resistance (< 50 Ω). The as-designed targets contribute to depositing SnO_2-based TCO films by magnetron sputtering.

Keywords: *SnO_2, Ta_2O_5, ZnO, Densification, Resistance.*

1. Introduction

Transparent conductive oxide (TCO) films are widely used in flat panel displays, solar cells, touch screens[1,2], and other fields due to their high transmittance in the visible region and low resistivity. The most commonly used TCO films are tin-doped indium oxide (ITO) films. Due to the high cost and toxicity of ITO films, low-cost ZnO and SnO_2 based TCO films have been proposed as alternatives. Amone them, SnO_2-based TCO films, such as SnO_2:F (FTO), SnO_2:Sb (ATO), have received increasing attention[3-6]. High-mobility Ta-doped SnO_2 (TTO) films with TiO_2 seed-layer were grown on glass substrate by pulsed laser deposition, which shows high mobility (83 $cm^2/V{\cdot}s$) and low resistivity (2.8×10^{-4} Ω·cm)[7]. However, the investigation of the TTO ceramic targets for magnetron sputtering should be further strengthened.

Nano oxide powders are pivotal for sintering dense ceramics, and the synthesis of fine SnO_2 powders primarily encompasses hydrothermal, fumed, electrolytic and Sol-Gel methods. The precursor prepared by $SnCl_4$ and ammonia was heated hydrothermally at 160 °C for 12 h to obtain SnO_2 nano powders[8]. The two-step vapor-phase oxidation process involves first Sn to SnO in a low-oxygen environment, and then further oxidizing SnO to SnO_2 in an oxygen-rich environment[9]. SnO_2 nanoparticles in a range of 25-150 nm were electrolytically synthesized under conditions of 60 V voltage and 0.06 M HCl, among which the particles with a size of 83.11 nm account for the highest proportion[10]. Additionally, nanocrystalline precursors were prepared via Sol-Gel method, and subsequently calcined at different temperatures to obtain SnO_2 nanoparticles with varying sizes[11]. These reports provide a foundation for the industrial synthesis of SnO_2 nano powders.

Pure SnO_2 ceramics with high resistivity are difficult to densification through sintering, and this difficulty is independent of sintering temperature[12]. Therefore, dopants are crucial for achieving densification and improving conductivity. Multiple sintering processes for ITO targets have been widely investigated[13], and these processes are also applicable to TTO targets. High density ATO targets with a relative density of 99.2% were obtained by spark plasma sintering (SPS) at 1000 °C[14]. Nearly fully dense FTO targets with a relative density of 98.5% were prepared by the SPS at temperatures ranging from 850 °C to 900 °C[15]. However, ATO targets sintered at 1250 °C in air exhibited lower density (95%)[16]. ZnO-SnO_2 binary ceramic targets sintered at 1600 °C had high density (99.78%), fine grains, and homogeneous structure[17]. Sn and Zn co-doped SnO_2 ceramics sintered at 1300 °C exhibited an enhancement of conductivity and density[18]. Furthermore, the Zn^{2+}, Ba^{3+}, Cu^{2+}, Nb^{5+}, Mn^{2+}, and Si^{4+} have been used to improve the conductivity of SnO_2-based ceramics[12,19-23]. These findings might offer new hope for further improving density and conductivity of SnO_2-based ceramics. However, researches on dense SnO_2-based targets doped with other elements and their sintering densification are still insufficient.

In this work, we enhanced the sintering behavior of 3 wt% Ta_2O_5 doped SnO_2 target by incorporating ZnO at contents of 0.7 wt%, 0.85 wt%, and 1.0 wt%. The phase structure, microstructure, density and resistance of the targets were investigated.

2. Experimental Procedures

High purity SnO_2 (99.99%), Ta_2O_5 (99.95%) and ZnO (99.95%) powders were used as raw materials. The Ta_2O_5 content in SnO_2 was fixed at 3 wt%. The ZnO doping contents were 0.7 wt%, 0.85 wt%, and 1.0 wt%, respectively. Thus, their corresponding targets were named T70, T85, and T10. The powders were dispersed with anhydrous ethanol in a ball milling tank, and the quality ratio of three types of zirconia

*e-mail: csuxjw@126.com

balls (8 mm, 4 mm, and 2 mm) was 3:2:1. The slurry with a solid content of 50% was mixed and milled at 410 rpm for 24 h, and then dried at 80 °C for 24 h. The powders were first sieved through a 150-mesh sieve, and then added an aqueous solution with 3 wt% polyvinyl alcohol (PVA) and 2 wt% polyethylene glycol (PEG) as binder. The mixture of powders and binder was granulated by an 80-mesh sieve. The granulated powders were pressed into discs with a diameter of 13 mm and a thickness of 2 mm. The green bodies with a relative density of about 55% were dewaxed at 600 °C for 3 h, and then sintered at 1350 °C, 1400 °C, 1450 °C, 1500 °C and 1550 °C for 4 h, and the rate of heating process is 2 °C/min.

X-ray diffraction (XRD, D8 Advance, Bruker) studied phase structure. Scanning electron microscopy (FE-SEM, Tecnai-450, FEI) observed microstructure and the elemental distribution. The average grain size of targets was statistically analyzed using Nano measure software. The density of targets was tested by the Archimedes method, and the theoretical density used in this work is 6.988 g/cm^3. The resistance of targets was measured by a multimeter (VC9205, Beicheng).

3. Results and Discussion

The morphologies of SnO_2 and Ta_2O_5 and ZnO powders, as depicted in Figure 1, reveal that SnO_2 powders are at the nanoscale, while Ta_2O_5 and ZnO powders have submicron size. The mixed powders containing 0.85 wt% ZnO are well-dispersed and finely milled through the ball-milling process, which can enhance sintering densification and promote uniform properties. Figure 2 shows physical images of the undoped TTO targets sintered at different temperatures. It is evident that the TTO targets without ZnO additive illustrate minimal shrinkage in the temperature range of 1350-1500 °C. Consequently, Ta_2O_5 does not function as sintering aid for SnO_2 ceramic, and the difficulty of sintering densification is the same as pure SnO_2 ceramics[24].

Figure 3 shows the XRD pattern of the ZnO doped TTO targets sintered at different temperatures. In Fig. 3(a), we observe three prominent diffraction peaks corresponding to the (110), (101) and (211) planes, with no visible peaks from impurity phases. This indicates that the rutile structure has formed, suggesting that the Zn and Ta have successfully integrated into the lattice of SnO_2 matrix[25,26]. Furthermore, as depicted in Fig. 3(b) and Fig. 3(c), increasing ZnO content to 0.85 wt% and 1.0 wt% still maintains the rutile structure of the TTO targets, again without any signs of impurity phase.

Figure 4 and Figure 5 shows the surface and cross-sectional morphologies of the T70 targets sintered at different temperatures. It is evident from Fig. 4 that the TTO targets possess a dense microstructure characterized by tightly packed grains and distinct grain boundaries. As depicted in Fig. 5, as the sintering temperature increases, the pores

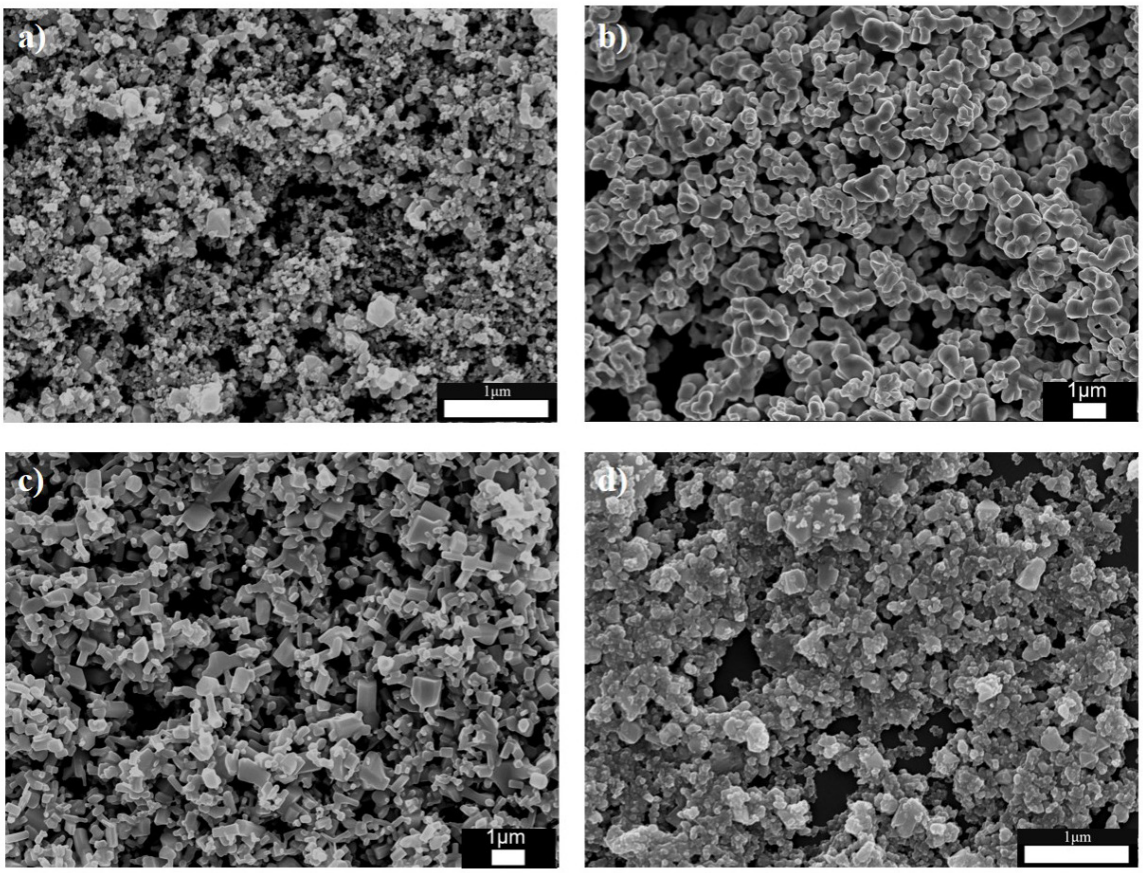

Figure 1. Microstructures of (a) SnO_2, (b) Ta_2O_5 and (c) ZnO powders and (d) mixed powders.

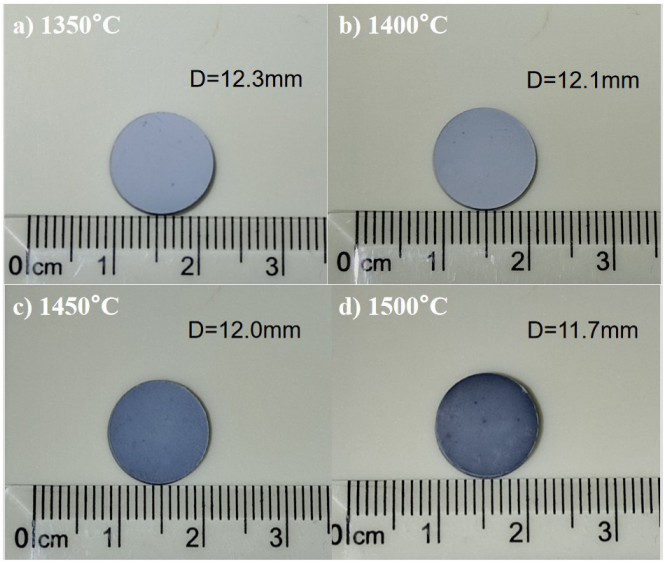

Figure 2. Diameters of the TTO targets without ZnO additive sintered at different temperatures.

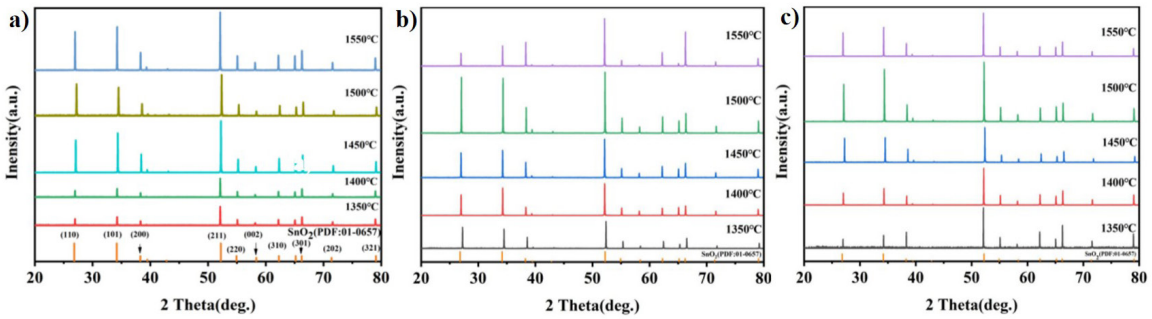

Figure 3. XRD patterns of (a) T70, (b) T85 and (c) T10 targets sintered at different temperatures.

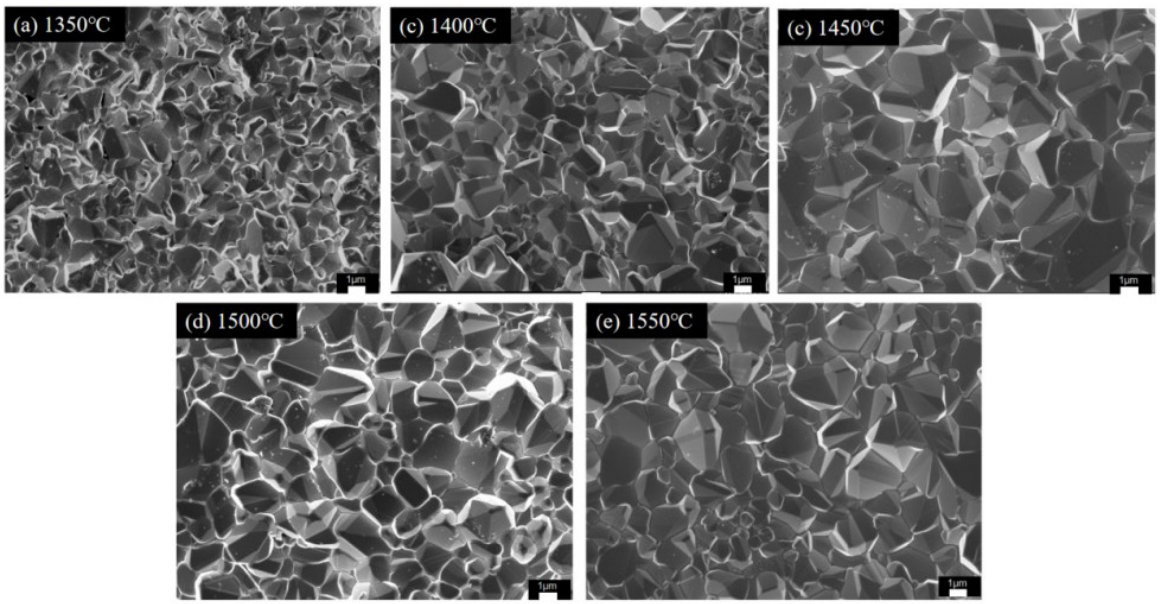

Figure 4. Surface morphologies of the T70 targets sintered at different temperatures.

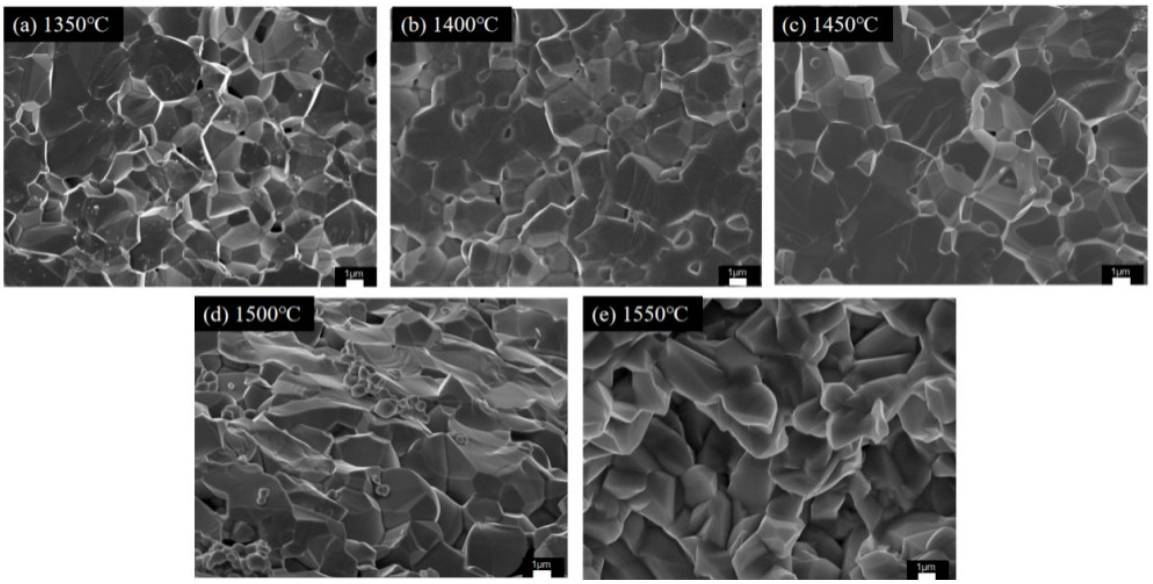

Figure 5. Cross-sectional morphologies of the T70 targets sintered at different temperatures.

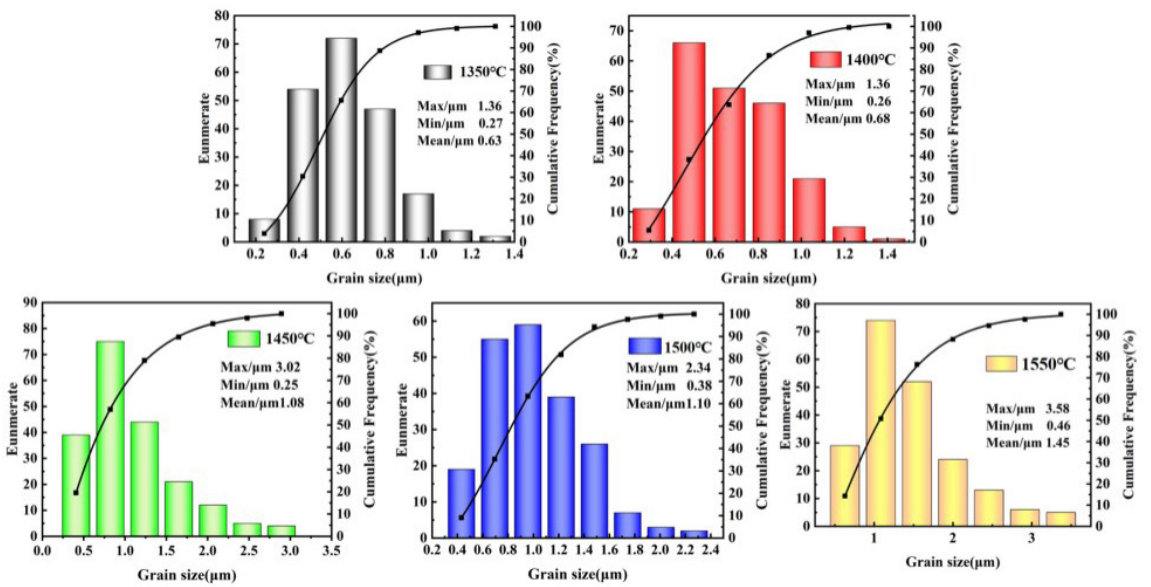

Figure 6. Grain size distribution of the T70 targets sintered at different temperatures.

within targets diminish in both size and number, indicating a corresponding rise in density. It is well known that pure SnO_2 ceramics are difficult to sinter densification, so ZnO can promote sintering densification[27]. Furthermore, fractures along grain boundaries are discernible. The grain size expands progressively with higher sintering temperatures[28]. The grain size distribution as shown in Figure 6 indicates that the targets have fine and uniform grains, and the grain size increases from 0.63 μm to 1.45 μm with increasing sintering temperature from 1350 °C to 1550 °C.

The surface (Figure 7, Figure 8) and cross-sectional (Figure 9, Figure 10) morphologies of the T85 and T10 targets demonstrate that these targets also exhibit a dense structure, tightly packed grains, clear grain boundaries and intergranular fracture. Higher sintering temperature further enhances grain growth and overall densification. The grain distribution depicted in Figure 11 underscores the uniformity of grain distribution within these targets. Specifically, as the sintering temperature rises, the average grain size of the T85 targets increases from 0.63 μm to 1.45 μm. However, the grain size of the T10 experiences a more modest increase, from 1.08 μm to 1.28 μm.

The microstructure in Figure 12 presents a large number of pores, indicating that the TTO targets have undergone

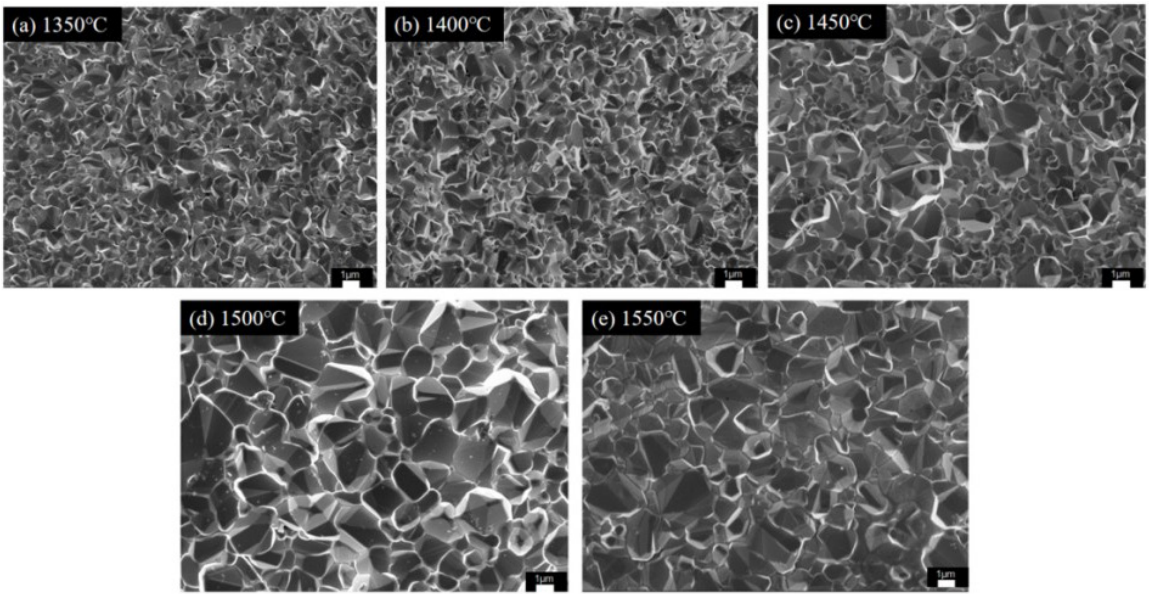

Figure 7. Surface morphologies of the T85 targets sintered at different temperatures.

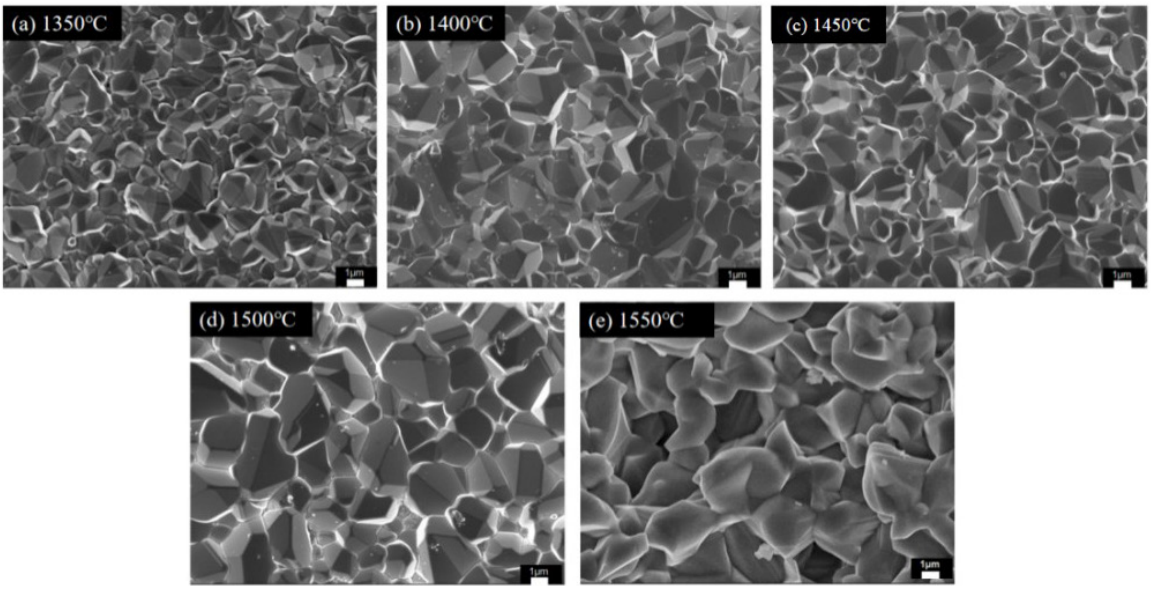

Figure 8. Surface morphologies of the T10 targets sintered at different temperatures.

over-sintering. When the TTO targets were sintered at 1600°C, the SnO_2 and ZnO components decomposed and evaporated, which is detrimental to achieving a higher density[29]. Figure 13 illustrates the elemental distribution of the T85 target. It is evident that the Sn, Ta and Zn elements are uniformly distributed throughout the T85 target. This uniform distribution contributes to improving the uniformity of density and conductivity in large-sized targets.

Figure 14 displays the density of the ZnO doped TTO targets sintered at various temperatures. It is evident that the density of all three types of TTO targets increases with both increasing ZnO content and sintering temperature. An optimal relative density of the ZnO doped TTO targets sintered at 1500 °C increases from 97.6% for the T70 to 99.9% for the T85, and then decrease to 98.8% for the T10. However, further increasing sintering temperature results in a decrease in density, which is attributed to the decomposition and volatilization of components. Therefore, ZnO can effectively promote the sintering densification of SnO_2-based ceramic targets[30]. On the other hand, due to the volatility of ZnO, excessive doping is not conducive to further increasing density.

Figure 15 displays the resistance of the ZnO doped TTO targets sintered at various temperatures. It is evident that the resistance gradually decreases with increasing sintering temperature, and

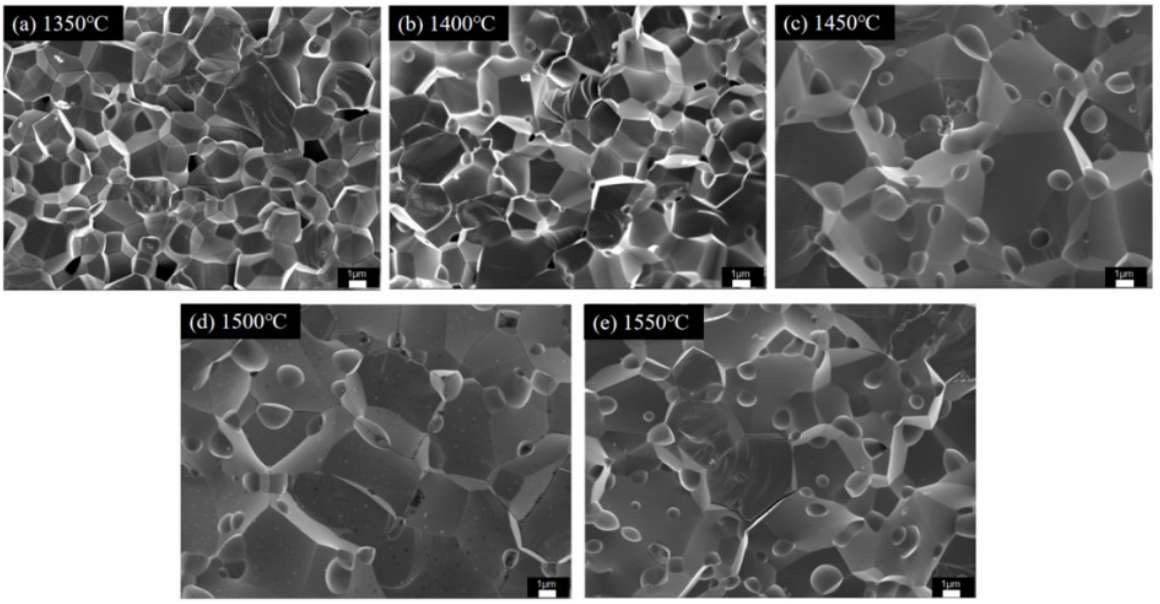

Figure 9. Cross-sectional morphologies of the T85 targets sintered at different temperatures.

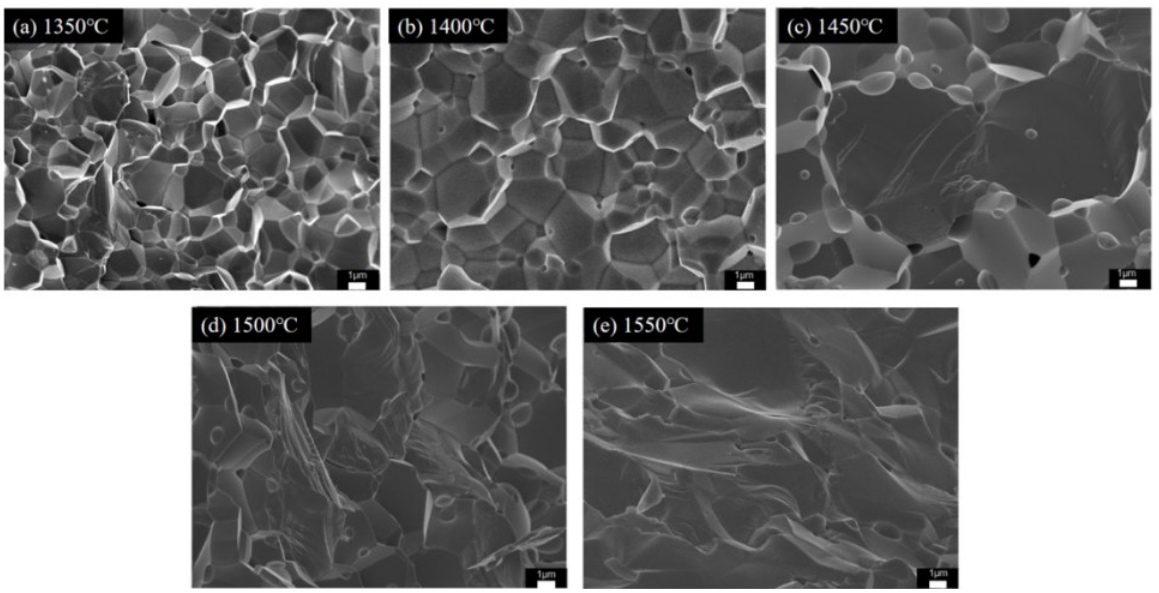

Figure 10. Cross-sectional morphologies of the T10 targets sintered at different temperatures.

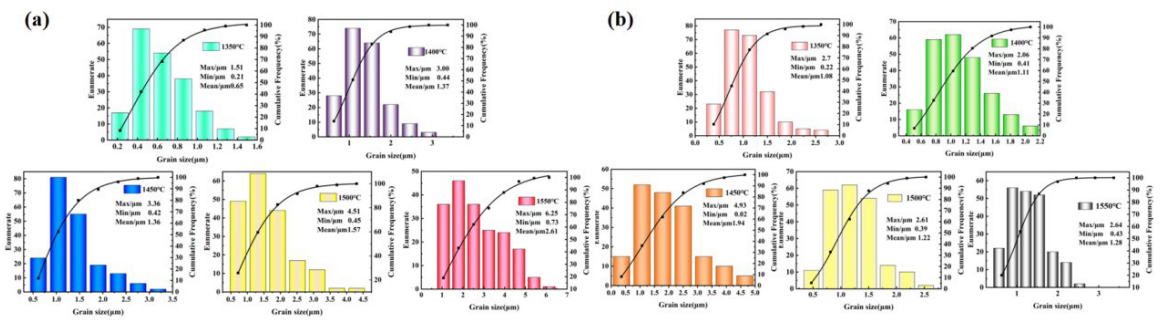

Figure 11. Grain size distribution of (a) T85 and (b) T10 targets sintered at different temperatures.

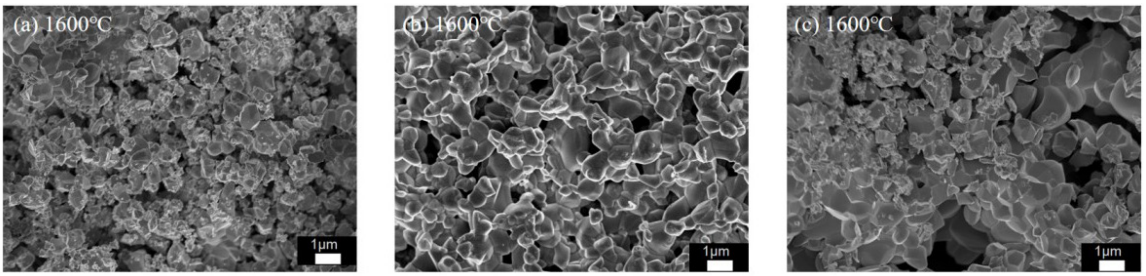

Figure 12. Surface morphologies of (a) T70 (b) T85, and (c) T10 targets sintered at 1600 °C.

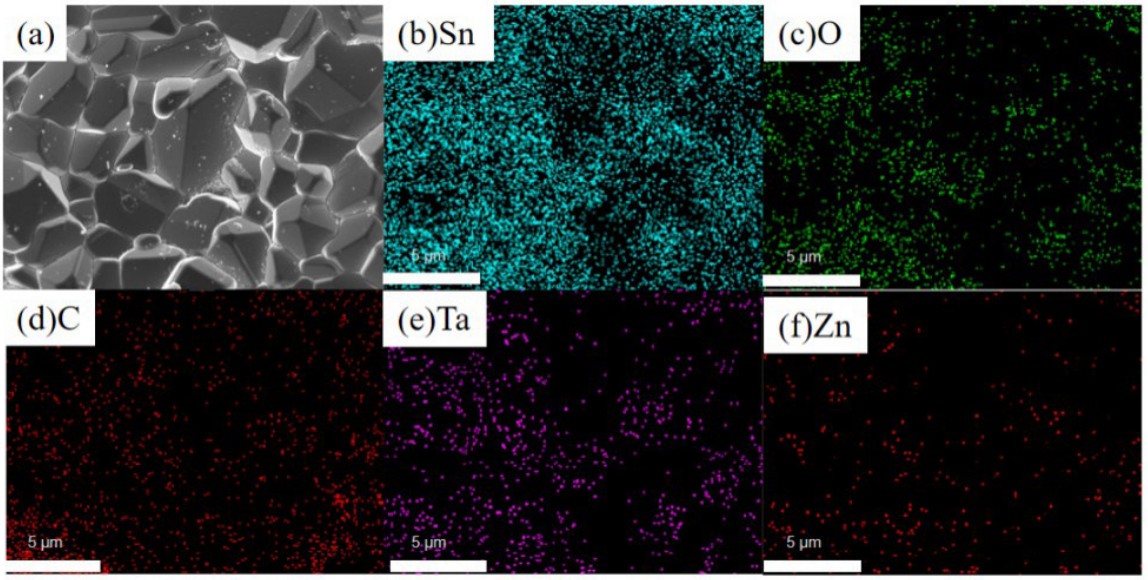

Figure 13. (a) Cross-sectional morphology and EDS mapping of (b) Sn, (c) O, (d) C, (e) Ta and (f) Zn in the T85 target sintered at 1500 °C.

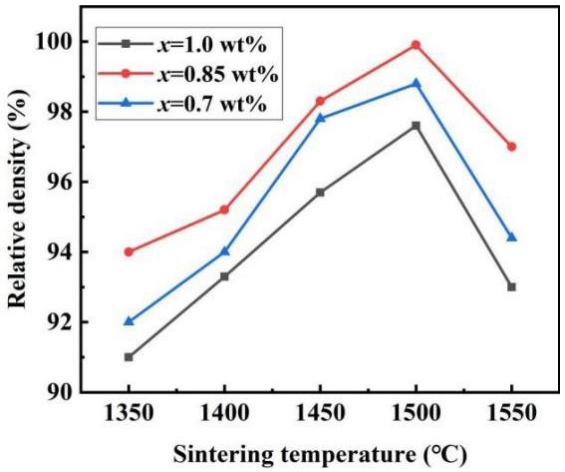

Figure 14. Density of the ZnO doped TTO targets sintered at different temperatures.

an optimal value was obtained at 1500 °C. Notably, the ZnO doping content has a minimal impact on resistance. At a low sintering temperature of 1350 °C, the TTO targets exhibit high resistance due to their low density. Conversely, at high sintering temperatures, the decomposition and volatilization of ZnO and SnO_2 lead to a decrease in density[31], also resulting in suboptimal

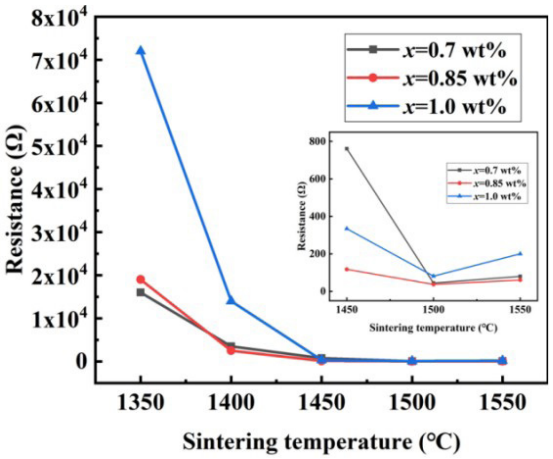

Figure 15. Resistance of the ZnO doped TTO targets sintered at different temperatures.

resistance values. The resistance decreases from 44 Ω for the T70 to 36 Ω for the T85, and then increase to 81 Ω for the T10. Consequently, the optimum sintering temperature for the ZnO doped TTO targets is below 1500 °C.

4. Conclusion

In this work, SnO_2-based targets for low-cost TCO film application were modified by doping 3 wt% Ta_2O_5 and different ZnO contents (0.7 wt%, 0.85 wt%, and 1.0 wt%). All the TTO targets exhibited a single rutile structure without impurity phases. The sintering densification was significantly improved by ZnO additive. The targets featured a dense microstructure and fine grains, and their average grain size range is from 0.2 μm to 3 μm. Due to the decomposition and volatilization of SnO_2 and ZnO, the sintering temperatures above 1500 °C were not conducive to further increasing density. As the sintering temperature increased, the resistance gradually decreased and was insensitive to ZnO content. Therefore, the density of the T70, T85 and T10 targets is 97.6%, 99.9% and 98.8%, respectively, and their corresponding resistance is 44 Ω, 36 Ω and 81 Ω, respectively. The 0.85 wt% ZnO doped target sintered at 1500 °C illustrates an excellent property. The enhanced-density SnO_2-based targets effectively suppress abnormal discharging during sputtering and meet the conductivity requirements for direct current magnetron sputtering.

5. Acknowledgments

This work was financially supported by the Joint Fund of NSFC-Guangxi (U21A2065), the National Natural Science Foundation of China (62464004), Science and Technology Major Project of Guangxi (AA21077018).

6. References

1. Boscarino S, Crupi I, Mirabella S, Simone F, Terrasi A. TCO/Ag/TCO transparent electrodes for solar cells application. Appl Phys, A Mater Sci Process. 2014;116:1287-91.
2. Sarath babu R, Narasimha murthy Y, Vinoth S, Isaac RSR, Mohanraj P, Ganesh V, et al. Enhancement in optoelectronic properties of lanthanum co-doped CdO: zn thin films for TCO applications. Superlattices Microstruct. 2022;162:107097.
3. Ma T, Missous M, Pinter G, Zhong X, Ben Spencer A. Sustainable ITO films with reduced indium content deposited by AACVD. J Mater Chem C Mater Opt Electron Devices. 2022;10(2):579-89.
4. Sun Y, Lei F, Gao S, Pan B, Zhou J, Xie Y. Atomically thin tin dioxide sheets for efficient catalytic oxidation of carbon monoxide. Angew Chem Int Ed. 2013;52(40):10569-72.
5. Sharma S, Alex M, Schmitt D, Seo DK. . Preparation and electrochemical properties of nanoporous transparent antimony-doped tin oxide (ATO) coatings. J Mater Chem A Mater Energy Sustain. 2013;3(3):699-706.
6. Yu S, Li L, Lyu X, Zhang W. Preparation and investigation of nano-thick FTO/Ag/FTO multilayer transparent electrodes with high figure of merit. Sci Rep. 2016;6(1):20399.
7. Fukumoto M, Nakao S, Shigematsu K, Ogawa D, Morikawa K, Hirose Y, et al. High mobility approaching the intrinsic limit in Ta-doped SnO_2 films epitaxially grown on TiO_2 (001) substrates. Sci Rep. 2020;10(1):6844.
8. Baik N, Sakai G, Miura N, Yamazoe N. Preparation of stabilized nanosized tin oxide particles by hydrothermal treatment. J Am Ceram Soc. 2000;83(12):2983-7.
9. Miller TA, Bakrania SD, Perez C, Wooldridge MS. A new method for direct preparation of tin dioxide nanocomposite materials. J Mater Res. 2005;20(11):2977-87.
10. Kurniawan F, Rahmi R. Synthesis of SnO_2 nanoparticles by high potential electrolysis. Bull Chem React Eng Catal. 2017;12(2):281-6.
11. Yang H, Han S, Wang L, Kim I-J, Son Y-M. Preparation and characterization of indium-doped tin dioxide nanocrystalline powders. Mater Chem Phys. 1998;56(2):153-6.
12. Medvedovski E. Tin oxide-based ceramics of high density obtained by pressureless sintering. Ceram Int. 2017;43(11):8396-405.
13. Mei F, Qin K, Yuan T, Li R, Liu L, Chen L, et al. Effects of oxygen flow velocity on the sintering properties of ITO targets. J Mater Sci Mater Electron. 2017;28:14711-9.
14. Wu J, Chen F, Shen Q, Schoenung JM, Zhang L. Spark plasma sintering and densification mechanisms of antimony-doped tin oxide nanoceramics. J Nanomater. 2013;(1):561895.
15. He H, Wang Z, Li B, Chen J, Luo W, Yang Z, et al. Comparisons between the high-pressure SPS and routine SPS of dense YH_{2-x}. J Alloys Compd. 2024;1002:175416.
16. Zhang L, Wu J, Chen F, Li X, Schoenung JM, Shen Q. Spark plasma sintering of antimony-doped tin oxide (ATO) nanoceramics with high density and enhanced electrical conductivity. Journal of Asian Ceramic Societies. 2013;1(1):114-9.
17. Jiang X, Long S, Zhu G, Xu H, Song J, Zhang X, et al. Preparation following the cold sintering process and properties of the materials. Ceram Int. 2023;49(11):17797-805.
18. Kim D-K, Lee J-H, Heo Y-W, Lee HY, Kim J-J. Co-doping effect of Zn and Sb in SnO_2: valence stabilization of Sb and expanded solubility limit. Ceram Int. 2011;37(7):2723-6.
19. Zhao J, Ni J, Zhao X, Xiong Y. Preparation and characterization of transparent conductive zinc doped tin oxide thin films prepared by radio-frequency magnetron sputtering. Journal of Wuhan University of Technology-Mater. 2011;26(3):388-92.
20. Villarreal SG, Vázquez Duron DA, Pech-Canul MI, Hernández MB, Falcon-Franco L, Aguilar-Martínez JA. The beneficial effect of $BaTiO_3$ on the structure, microstructure, and electrical properties of SnO_2-based ceramics. Ceram Int. 2024;50(1):927-33.
21. Turgut G, Keskenler EF, Aydın S, Sönmez E, Doğan S, Düzgün B, et al. Effect of Nb doping on structural, electrical and optical properties of spray deposited SnO_2 thin films. Superlattices Microstruct. 2013;56:107-16.

22. Lee C-H, Nam B-A, Choi W-K, Lee J-K, Choi D-J, Oh Y-J. Mn: SnO_2 ceramics as p-type oxide semiconductor. Mater Lett. 2011;65(4):722-5.
23. Zur L, Lam TNT, Meneghetti M, Van Thi TT, Lukowiak A, Chiasera A, et al. Tin-dioxide nanocrystals as Er^{3+} luminescence sensitizers: formation of glass-ceramic thin films and their characterization. Opt Mater. 2017;63:95-100.
24. Mihaiu S, Toader A, Atkinson I, Mocioiu OC, Hornoiu C, Teodorescu VS, et al. Advanced ceramics in the SnO_2-ZnO binary system. Ceram Int. 2015;41(3):4936-45.
25. Wang T, Xu J, Zhu G, Shang F, Xu H. Sintering densification of ITO targets with low tin oxide content for depositing TCO films as electrodes of solar cells. Ceram Int. 2024;50(3):5532-40.
26. Bakar A, Afaq A, Latif S, Iftikhar A, Asif M. A comprehensive study of titanium-doped tin oxide rutile for structural and optical properties. Physica B. 2021;619:413210.
27. Šimonová P, Gregorová E, Pabst W. Young's modulus evolution during sintering and thermal cycling of pure tin oxide ceramics. J Eur Ceram Soc. 2021;41(15):7816-27.
28. Huai Z, Chen J, Qi C, Sun B, Liu S, Song H, et al. Sintering densification behavior of ZnO-SnO_2 binary ceramic targets. J Am Ceram Soc. 2023;106(1):259-73.
29. German RM. Sintering trajectories: description on how density, surface area, and grain size change. JOM. 2016;68:878-84.
30. Saadeddin I, Hilal HS, Pecquenard B, Marcus J, Mansouri A, Labrugere C, et al. Simultaneous doping of Zn and Sb in SnO_2 ceramics: enhancement of electrical conductivity. Solid State Sci. 2006;8(1):7-13.
31. Omata T, Kita M, Okada H, Otsuka-Yao-Matsuo S, Ono N, Ikawa H. Characterization of indium-tin oxide sputtering targets showing various densities of nodule formation. Thin Solid Films. 2006;503(1-2):22-8.